Chapter 5 (Cont.)

Modeling Flow conditions for a model test are completely similar if all relevant dimensionless parameters have the same corresponding values for the model and the prototype.

Geometric Similarity A model and prototype are *geometrically similar* if and only if all body dimensions in all three coordinates have the same linear-scale ratio.
All angles are preserved in geometric similarity. All flow directions are preserved. The orientations of model and prototype with respect to the surroundings must be identical.

Kinematic Similarity The motions of two systems are kinematically similar if homologous particles lie at homologous points at homologous times.

Dynamic Similarity Dynamic similarity exists when the model and the prototype have the same length-scale ratio, time-scale ratio, and force-scale (or mass-scale) ratio.

equivalence of Reynolds and Froude numbers can be achieved only by dramatic changes in fluid properties, whereas in fact most model testing is simply done with water or air, the cheapest fluids available.

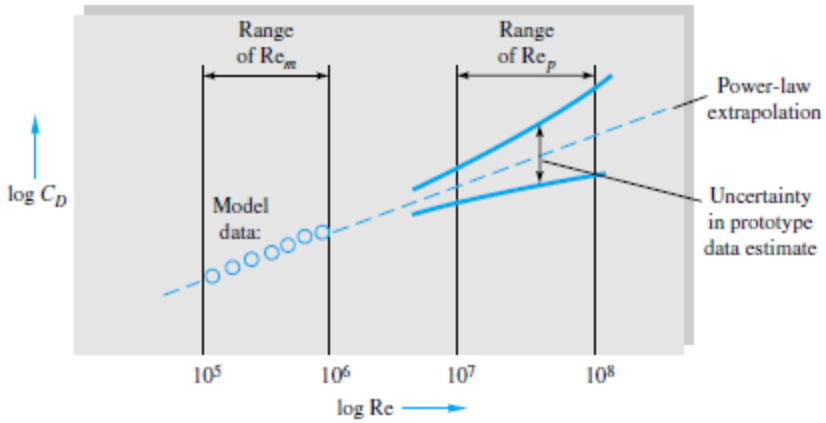

Fig. 5.8 Reynolds-number extrapolation, or scaling, of hydraulic data with equal Froude numbers.

Chapter 5 (Cont.)

Dimensionless Groups in Fluid Mechanics

Parameter	Definition	Qualitative ratio of effects	Importance
Reynolds number	$\mathrm{Re} = \frac{\rho U L}{\mu}$	$\frac{\text{Inertia}}{\text{Viscosity}}$	Always
Mach number	$\mathrm{Ma} = \frac{U}{a}$	$\frac{\text{Flow speed}}{\text{Sound speed}}$	Compressible flow
Froude number	$\mathrm{Fr} = \frac{U^2}{gL}$	$\frac{\text{Inertia}}{\text{Gravity}}$	Free-surface flow
Weber number	$\mathrm{We} = \frac{\rho U^2 L}{\Upsilon}$	$\frac{\text{Inertia}}{\text{Surface tension}}$	Free-surface flow
Cavitation number (Euler number)	$\mathrm{Ca} = \frac{p - p_v}{\rho U^2}$	$\frac{\text{Pressure}}{\text{Inertia}}$	Cavitation
Prandtl number	$\mathrm{Pr} = \frac{\mu c_p}{k}$	$\frac{\text{Dissipation}}{\text{Conduction}}$	Heat convection
Eckert number	$\mathrm{Ec} = \frac{U^2}{c_p T_0}$	$\frac{\text{Kinetic energy}}{\text{Enthalpy}}$	Dissipation
Specific-heat ratio	$k = \frac{c_p}{c_v}$	$\frac{\text{Enthalpy}}{\text{Internal energy}}$	Compressible flow
Strouhal number	$\mathrm{St} = \frac{\omega L}{U}$	$\frac{\text{Oscillation}}{\text{Mean speed}}$	Oscillating flow
Roughness ratio	$\frac{\epsilon}{L}$	$\frac{\text{Wall roughness}}{\text{Body length}}$	Turbulent, rough walls
Grashof number	$\mathrm{Gr} = \frac{\beta \Delta T g L^3 \rho^2}{\mu^2}$	$\frac{\text{Buoyancy}}{\text{Viscosity}}$	Natural convection
Temperature ratio	$\frac{T_w}{T_0}$	$\frac{\text{Wall temperature}}{\text{Stream temperature}}$	Heat transfer
Pressure coefficient	$C_p = \frac{p - p_\infty}{\frac{1}{2}\rho U^2}$	$\frac{\text{Static pressure}}{\text{Dynamic pressure}}$	Aerodynamics, hydrodynamics
Lift coefficient	$C_L = \frac{L}{\frac{1}{2}\rho U^2 A}$	$\frac{\text{Lift force}}{\text{Dynamic force}}$	Aerodynamics, hydrodynamics
Drag coefficient	$C_D = \frac{D}{\frac{1}{2}\rho U^2 A}$	$\frac{\text{Drag force}}{\text{Dynamic force}}$	Aerodynamics, hydrodynamics

Chapter 6

Reynolds-Number Regimes

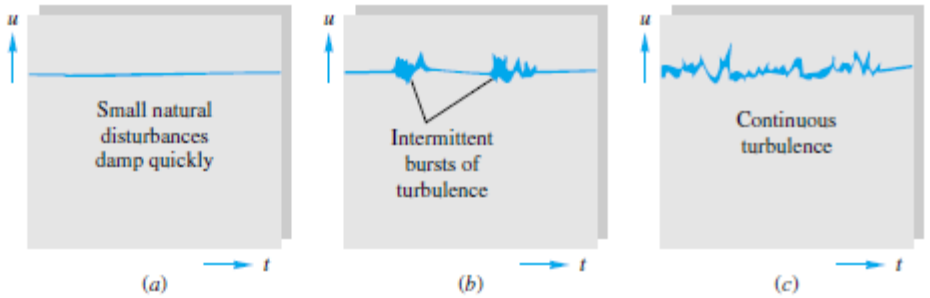

Fig. 6.1 The three regimes of viscous flow: (*a*) laminar flow at low Re; (*b*) transition at intermediate Re; (*c*) turbulent flow at high Re.

$0 < \mathrm{Re} < 1$: highly viscous laminar "creeping" motion

$1 < \mathrm{Re} < 100$: laminar, strong Reynolds-number dependence

$100 < \mathrm{Re} < 10^3$: laminar, boundary-layer theory useful

$10^3 < \mathrm{Re} < 10^4$: transition to turbulence

$10^4 < \mathrm{Re} < 10^6$: turbulent, moderate Reynolds-number dependence

$10^6 < \mathrm{Re} < \infty$: turbulent, slight Reynolds-number dependence

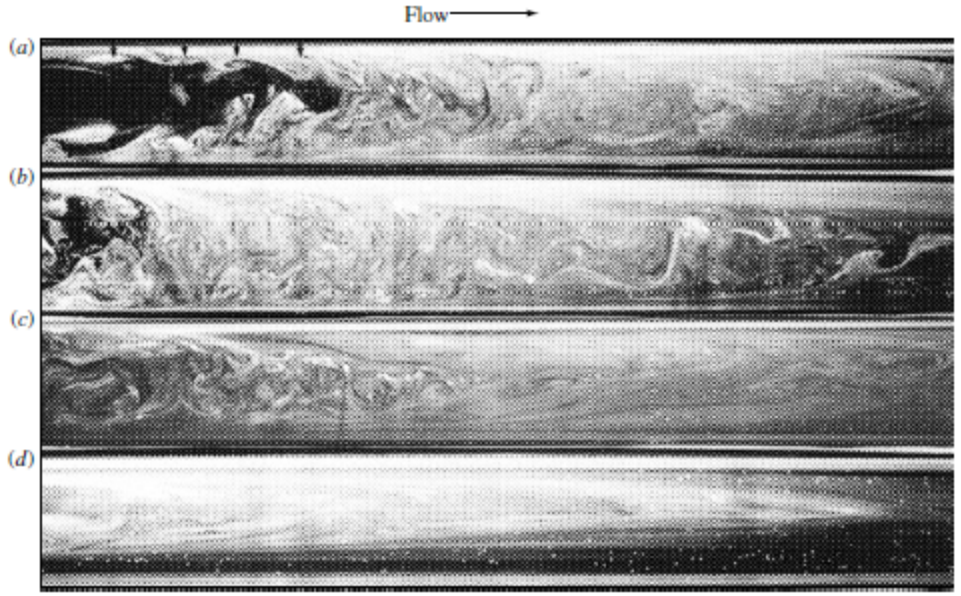

Fig. 6.3 Formation of a turbulent puff in pipe flow: (*a*) and (*b*) near the entrance; (*c*) somewhat downstream; (*d*) far downstream. *(From Ref. 45, courtesy of P. R. Bandyopadhyay.)*

Chapter 6

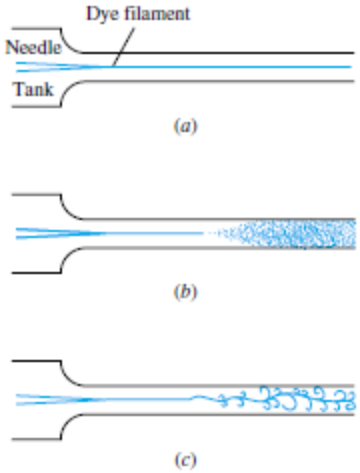

Fig. 6.5 Reynolds' sketches of pipe-flow transition: (*a*) low-speed, laminar flow; (*b*) high-speed, turbulent flow; (*c*) spark photograph of condition (*b*). (*From Ref. 4.*)

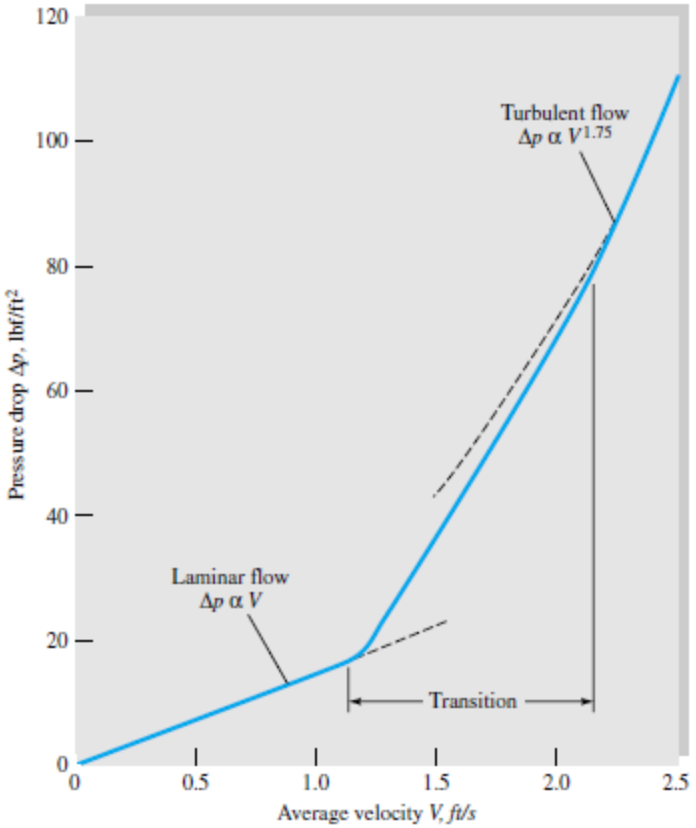

Fig. 6.4 Experimental evidence of transition for water flow in a $\frac{1}{4}$-in smooth pipe 10 ft long.

$$Re_{d,crit} \approx 2300$$

Chapter 6

Dimensional analysis shows that the Reynolds number is the only parameter affecting entrance length. If

$$L_e = f(d, V, \rho, \mu) \qquad V = \frac{Q}{A}$$

then

$$\frac{L_e}{d} = g\left(\frac{\rho V d}{\mu}\right) = g(\mathrm{Re}) \tag{6.4}$$

For laminar flow [2, 3], the accepted correlation is

$$\frac{L_e}{d} \approx 0.06\ \mathrm{Re} \qquad \text{laminar} \tag{6.5}$$

The maximum laminar entrance length, at $\mathrm{Re}_{d,\mathrm{crit}} = 2300$, is $L_e = 138d$, which is the longest development length possible.

In turbulent flow the boundary layers grow faster, and L_e is relatively shorter, according to the approximation for smooth walls

$$\frac{L_e}{d} \approx 4.4\ \mathrm{Re}_d^{1/6} \qquad \text{turbulent} \tag{6.6}$$

Re_d	4000	10^4	10^5	10^6	10^7	10^8
L_e/d	18	20	30	44	65	95

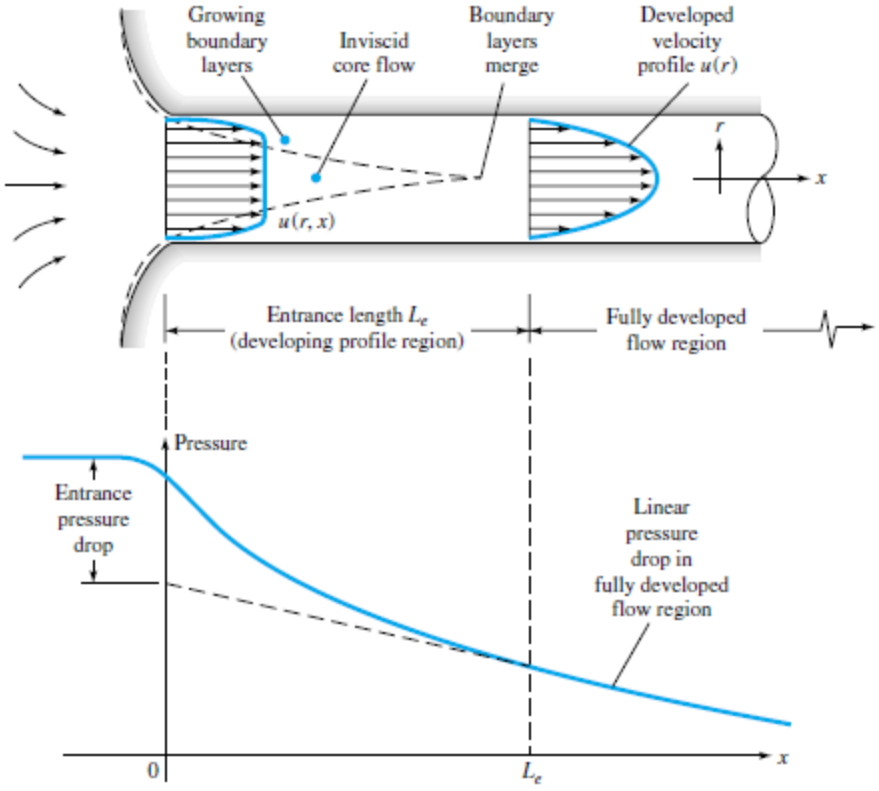

Fig. 6.6 Developing velocity profiles and pressure changes in the entrance of a duct flow.

Chapter 6

Reynolds' Time-Averaging Concept

$$\bar{u} = \frac{1}{T}\int_0^T u\,dt$$

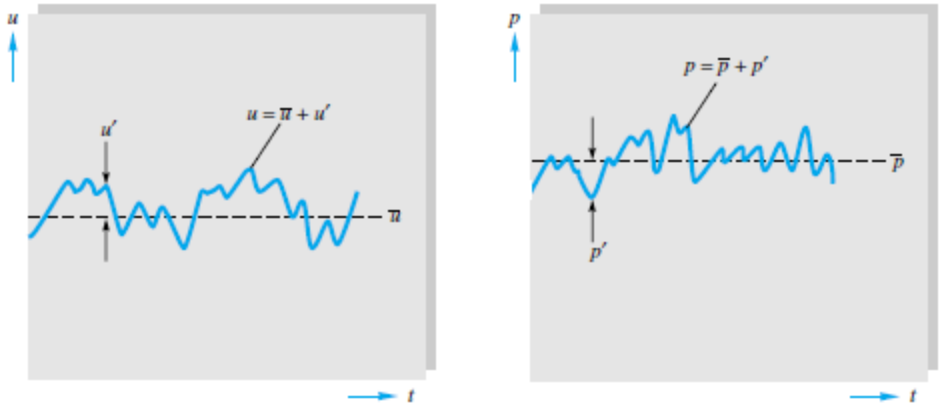

Fig. 6.7 Definition of mean and fluctuating turbulent variables: (*a*) velocity; (*b*) pressure.

Momentum:

$$\rho\frac{d\mathbf{V}}{dt} = -\nabla p + \rho\mathbf{g} + \mu\nabla^2\mathbf{V}$$

$$\rho\frac{d\bar{u}}{dt} = -\frac{\partial\bar{p}}{\partial x} + \rho g_x + \frac{\partial}{\partial x}\left(\mu\frac{\partial\bar{u}}{\partial x} - \rho\overline{u'^2}\right) + \frac{\partial}{\partial y}\left(\mu\frac{\partial\bar{u}}{\partial y} - \rho\overline{u'v'}\right) + \frac{\partial}{\partial z}\left(\mu\frac{\partial\bar{u}}{\partial z} - \rho\overline{u'w'}\right) \tag{6.14}$$

The three correlation terms $-\rho\overline{u'^2}$, $-\rho\overline{u'v'}$, and $-\rho\overline{u'w'}$ are called *turbulent stresses*

Fortunately, in duct and boundary-layer flow, the stress $-\rho\overline{u'v'}$ associated with direction y normal to the wall is dominant, and we can approximate with excellent accuracy a simpler streamwise momentum equation

$$\rho\frac{d\bar{u}}{dt} \approx -\frac{\partial\bar{p}}{\partial x} + \rho g_x + \frac{\partial\tau}{\partial y} \tag{6.15}$$

where

$$\tau = \mu\frac{\partial\bar{u}}{\partial y} - \rho\overline{u'v'} = \tau_{\text{lam}} + \tau_{\text{turb}} \tag{6.16}$$

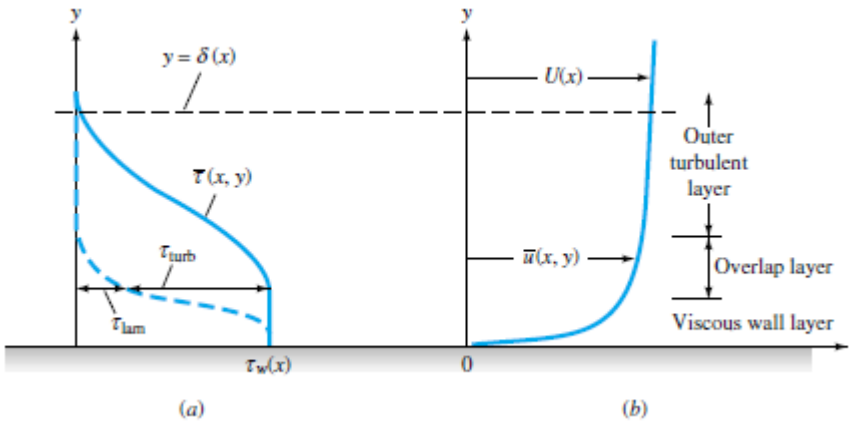

Fig. 6.8 Typical velocity and shear distributions in turbulent flow near a wall: (*a*) shear; (*b*) velocity.

Chapter 6

The Logarithmic-Overlap Law We have seen in Fig. 6.8 that there are three regions in turbulent flow near a wall:

1. Wall layer: Viscous shear dominates.
2. Outer layer: Turbulent shear dominates.
3. Overlap layer: Both types of shear are important.

For the wall layer, Prandtl deduced in 1930 that u must be independent of the shear-layer thickness

$$u = f(\mu, \tau_w, \rho, y) \tag{6.17}$$

By dimensional analysis, this is equivalent to

$$u^+ = \frac{u}{u^*} = F\left(\frac{yu^*}{\nu}\right) \qquad u^* = \left(\frac{\tau_w}{\rho}\right)^{1/2} \tag{6.18}$$

Equation (6.18) is called the *law of the wall,* and the quantity u^* is termed the *friction velocity* because it has dimensions $\{LT^{-1}\}$, although it is not actually a flow velocity.

Subsequently, Kármán in 1933 deduced that u in the outer layer is independent of molecular viscosity, but its deviation from the stream velocity U must depend on the layer thickness δ and the other properties

$$(U - u)_{\text{outer}} = g(\delta, \tau_w, \rho, y) \tag{6.19}$$

Again, by dimensional analysis we rewrite this as

$$\frac{U - u}{u^*} = G\left(\frac{y}{\delta}\right) \tag{6.20}$$

where u^* has the same meaning as in Eq. (6.18). Equation (6.20) is called the *velocity-defect law* for the outer layer.

Both the wall law (6.18) and the defect law (6.20) are found to be accurate for a wide variety of experimental turbulent duct and boundary-layer flows [1 to 3]. They are different in form, yet they must overlap smoothly in the intermediate layer. In 1937 C. B. Millikan showed that this can be true only if the overlap-layer velocity varies logarithmically with y:

$$\frac{u}{u^*} = \frac{1}{\kappa} \ln \frac{yu^*}{\nu} + B \qquad \text{overlap layer} \tag{6.21}$$

Over the full range of turbulent smooth wall flows, the dimensionless constants κ and B are found to have the approximate values $\kappa \approx 0.41$ and $B \approx 5.0$. Equation (6.21) is called the *logarithmic-overlap layer.*

Thus by dimensional reasoning and physical insight we infer that a plot of u versus $\ln y$ in a turbulent-shear layer will show a curved wall region, a curved outer region, and a straight-line logarithmic overlap. Figure 6.9 shows that this is exactly the case. The four outer-law profiles shown all merge smoothly with the logarithmic-overlap law but have different magnitudes because they vary in external pressure gradient. The wall law is unique and follows the linear viscous relation

$$u^+ = \frac{u}{u^*} = \frac{yu^*}{\nu} = y^+ \tag{6.22}$$

from the wall to about $y^+ = 5$, thereafter curving over to merge with the logarithmic law at about $y^+ = 30$.

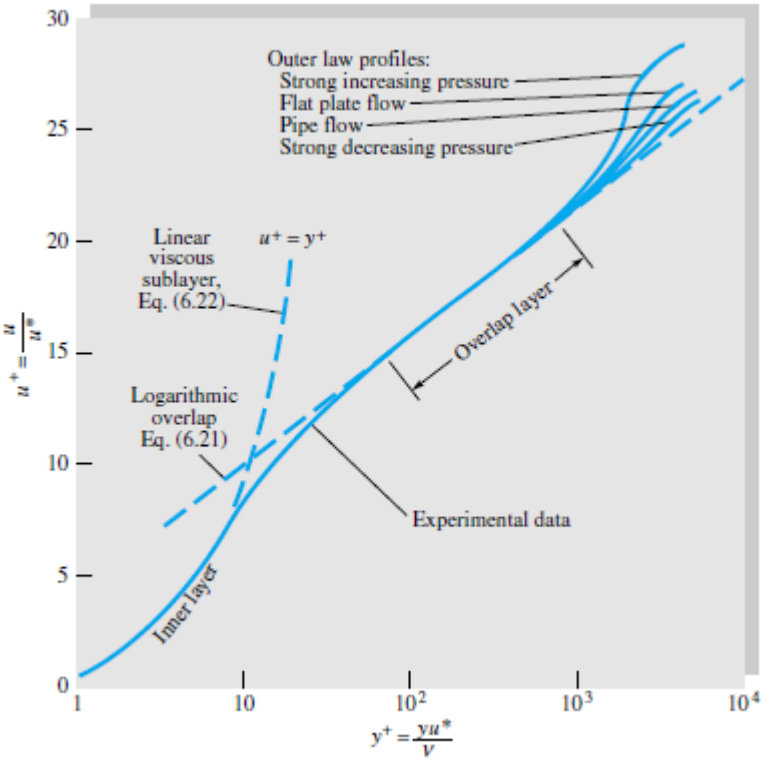

Fig. 6.9 Experimental verification of the inner-, outer-, and overlap-layer laws relating velocity profiles in turbulent wall flow.

Chapter 6

Flow in a Circular Pipe

The continuity relation, Eq. (3.23), reduces to

$$Q_1 = Q_2 = \text{const}$$

or

$$V_1 = \frac{Q_1}{A_1} = V_2 = \frac{Q_2}{A_2} \tag{6.23}$$

since the pipe is of constant area. The steady-flow energy equation (3.71) reduces to

$$\frac{p_1}{\rho} + \frac{1}{2}\alpha_1 V_1^2 + gz_1 = \frac{p_2}{\rho} + \frac{1}{2}\alpha_2 V_2^2 + gz_2 + gh_f \tag{6.24}$$

$$h_f = \left(z_1 + \frac{p_1}{\rho g}\right) - \left(z_2 + \frac{p_2}{\rho g}\right) = \Delta\left(z + \frac{p}{\rho g}\right) = \Delta z + \frac{\Delta p}{\rho g} \tag{6.25}$$

Finally apply the momentum relation (3.40) to the control volume in Fig. 6.10, accounting for applied forces due to pressure, gravity, and shear

$$\Delta p\ \pi R^2 + \rho g(\pi R^2)\ \Delta L \sin\phi - \tau_w(2\pi R)\ \Delta L = \dot{m}(V_2 - V_1) = 0 \tag{6.26}$$

This equation relates h_f to the wall shear stress

$$\Delta z + \frac{\Delta p}{\rho g} = h_f = \frac{2\tau_w}{\rho g}\frac{\Delta L}{R} \tag{6.27}$$

where we have substituted $\Delta z = \Delta L \sin\phi$ from Fig. 6.10.

So far we have not assumed either laminar or turbulent flow. If we can correlate τ_w with flow conditions, we have solved the problem of head loss in pipe flow. Functionally, we can assume that

$$\tau_w = F(\rho, V, \mu, d, \epsilon) \tag{6.28}$$

where ϵ is the wall-roughness height. Then dimensional analysis tells us that

$$\frac{8\tau_w}{\rho V^2} = f = F\left(\text{Re}_d, \frac{\epsilon}{d}\right) \tag{6.29}$$

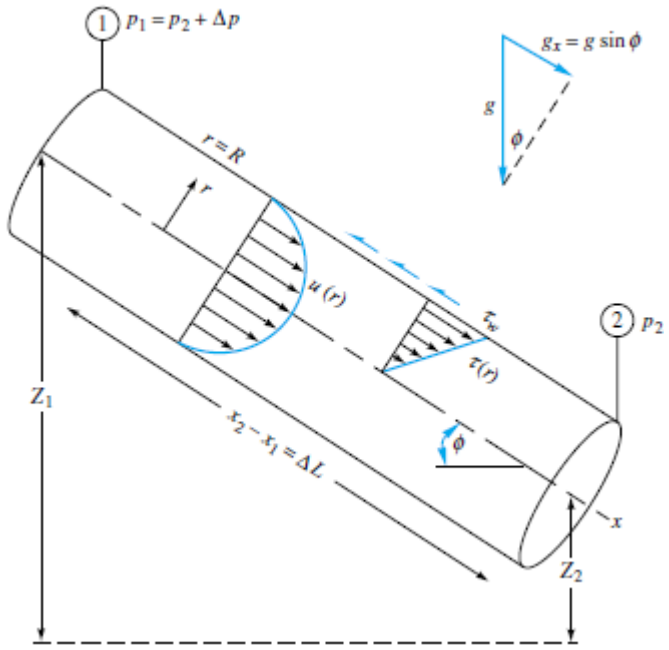

Fig. 6.10 Control volume of steady, fully developed flow between two sections in an inclined pipe.

Combining Eqs. (6.27) and (6.29), we obtain the desired expression for finding pipe-head loss

$$h_f = f\frac{L}{d}\frac{V^2}{2g} \tag{6.30}$$

This is the *Darcy-Weisbach equation*, valid for duct flows of any cross section and for laminar and turbulent flow. It was proposed by Julius Weisbach, a German professor who in 1850 published the first modern textbook on hydrodynamics.

Chapter 6

Equations of Motion

For either laminar or turbulent flow, the continuity equation in cylindrical coordinates is given by (App. D)

$$\frac{1}{r}\frac{\partial}{\partial r}(rv_r) + \frac{1}{r}\frac{\partial}{\partial \theta}(v_\theta) + \frac{\partial u}{\partial x} = 0 \tag{6.31}$$

We assume that there is no swirl or circumferential variation, $v_\theta = \partial/\partial\theta = 0$, and fully developed flow: $u = u(r)$ only. Then Eq. (6.31) reduces to

$$\frac{1}{r}\frac{\partial}{\partial r}(rv_r) = 0$$

or

$$rv_r = \text{const} \tag{6.32}$$

But at the wall, $r = R$, $v_r = 0$ (no slip); therefore (6.32) implies that $v_r = 0$ everywhere. Thus in fully developed flow there is only one velocity component, $u = u(r)$.

The momentum differential equation in cylindrical coordinates now reduces to

$$\rho u\frac{\partial u}{\partial x} = -\frac{dp}{dx} + \rho g_x + \frac{1}{r}\frac{\partial}{\partial r}(r\tau) \tag{6.33}$$

where τ can represent either laminar or turbulent shear. But the left-hand side vanishes because $u = u(r)$ only. Rearrange, noting from Fig. 6.10 that $g_x = g \sin \phi$:

$$\frac{1}{r}\frac{\partial}{\partial r}(r\tau) = \frac{d}{dx}(p - \rho g x \sin\phi) = \frac{d}{dx}(p + \rho g z) \tag{6.34}$$

Since the left-hand side varies only with r and the right-hand side varies only with x, it follows that both sides must be equal to the same constant.[2] Therefore we can integrate Eq. (6.34) to find the shear distribution across the pipe, utilizing the fact that $\tau = 0$ at $r = 0$

$$\tau = \frac{1}{2}r\frac{d}{dx}(p + \rho g z) = (\text{const})(r) \tag{6.35}$$

Thus the shear varies linearly from the centerline to the wall, for either laminar or turbulent flow. This is also shown in Fig. 6.10. At $r = R$, we have the wall shear

$$\tau_w = \frac{1}{2}R\frac{\Delta p + \rho g\,\Delta z}{\Delta L} \tag{6.36}$$

which is identical with our momentum relation (6.27). We can now complete our study of pipe flow by applying either laminar or turbulent assumptions to fill out Eq. (6.35).

Chapter 6

Laminar-Flow Solution

Note in Eq. (6.35) that the HGL slope $d(p + \rho gz)/dx$ is *negative* because both pressure and height drop with x. For laminar flow, $\tau = \mu\, du/dr$, which we substitute in Eq. (6.35)

$$\mu \frac{du}{dr} = \frac{1}{2} rK \qquad K = \frac{d}{dx}(p + \rho gz) \tag{6.37}$$

Integrate once

$$u = \frac{1}{4} r^2 \frac{K}{\mu} + C_1 \tag{6.38}$$

The constant C_1 is evaluated from the no-slip condition at the wall: $u = 0$ at $r = R$

$$0 = \frac{1}{4} R^2 \frac{K}{\mu} + C_1 \tag{6.39}$$

or $C_1 = -\frac{1}{4}R^2K/\mu$. Introduce into Eq. (6.38) to obtain the exact solution for laminar fully developed pipe flow

$$u = \frac{1}{4\mu}\left[-\frac{d}{dx}(p + \rho gz)\right](R^2 - r^2) \tag{6.40}$$

The laminar-flow profile is thus a paraboloid falling to zero at the wall and reaching a maximum at the axis

$$u_{\max} = \frac{R^2}{4\mu}\left[-\frac{d}{dx}(p + \rho gz)\right] \tag{6.41}$$

It resembles the sketch of $u(r)$ given in Fig. 6.10.

The laminar distribution (6.40) is called *Hagen-Poiseuille flow* to commemorate the experimental work of G. Hagen in 1839 and J. L. Poiseuille in 1940, both of whom established the pressure-drop law, Eq. (6.1). The first theoretical derivation of Eq. (6.40) was given independently by E. Hagenbach and by F. Neumann around 1859.

Other pipe-flow results follow immediately from Eq. (6.40). The volume flow is

$$Q = \int_0^R u\, dA = \int_0^R u_{\max}\left(1 - \frac{r^2}{R^2}\right) 2\pi r\, dr$$

$$= \frac{1}{2} u_{\max} \pi R^2 = \frac{\pi R^4}{8\mu}\left[-\frac{d}{dx}(p + \rho gz)\right] \tag{6.42}$$

Thus the average velocity in laminar flow is one-half the maximum velocity

$$V = \frac{Q}{A} = \frac{Q}{\pi R^2} = \frac{1}{2} u_{\max} \tag{6.43}$$

For a horizontal tube ($\Delta z = 0$), Eq. (6.42) is of the form predicted by Hagen's experiment, Eq. (6.1):

$$\Delta p = \frac{8\mu LQ}{\pi R^4} \tag{6.44}$$

The wall shear is computed from the wall velocity gradient

$$\tau_w = \left|\mu \frac{du}{dr}\right|_{r=R} = \frac{2\mu u_{\max}}{R} = \frac{1}{2} R \left|\frac{d}{dx}(p + \rho gz)\right| \tag{6.45}$$

This gives an exact theory for laminar Darcy friction factor

$$f = \frac{8\tau_w}{\rho V^2} = \frac{8(8\mu V/d)}{\rho V^2} = \frac{64\mu}{\rho V d}$$

or

$$f_{\text{lam}} = \frac{64}{\text{Re}_d} \tag{6.46}$$

This is plotted later in the Moody chart (Fig. 6.13). The fact that f drops off with increasing Re_d should not mislead us into thinking that shear decreases with velocity: Eq. (6.45) clearly shows that τ_w is proportional to $u_{\max}$; it is interesting to note that τ_w is independent of density because the fluid acceleration is zero.

The laminar head loss follows from Eq. (6.30)

$$h_{f,\text{lam}} = \frac{64\mu}{\rho V d} \frac{L}{d} \frac{V^2}{2g} = \frac{32\mu LV}{\rho g d^2} = \frac{128\mu LQ}{\pi \rho g d^4} \tag{6.47}$$

We see that laminar head loss is proportional to V.

Chapter 6

Turbulent-Flow Solution

For turbulent pipe flow we need not solve a differential equation but instead proceed with the logarithmic law, as in Example 6.3. Assume that Eq. (6.21) correlates the local mean velocity $u(r)$ all the way across the pipe

$$\frac{u(r)}{u^*} \approx \frac{1}{\kappa} \ln \frac{(R-r)u^*}{\nu} + B \tag{6.48}$$

where we have replaced y by $R - r$. Compute the average velocity from this profile

$$V = \frac{Q}{A} = \frac{1}{\pi R^2} \int_0^R u^* \left[\frac{1}{\kappa} \ln \frac{(R-r)u^*}{\nu} + B \right] 2\pi r \, dr$$

$$= \frac{1}{2} u^* \left(\frac{2}{\kappa} \ln \frac{Ru^*}{\nu} + 2B - \frac{3}{\kappa} \right) \tag{6.49}$$

Introducing $\kappa = 0.41$ and $B = 5.0$, we obtain, numerically,

$$\frac{V}{u^*} \approx 2.44 \ln \frac{Ru^*}{\nu} + 1.34 \tag{6.50}$$

This looks only marginally interesting until we realize that V/u^* is directly related to the Darcy friction factor

$$\frac{V}{u^*} = \left(\frac{\rho V^2}{\tau_w} \right)^{1/2} = \left(\frac{8}{f} \right)^{1/2} \tag{6.51}$$

Moreover, the argument of the logarithm in (6.50) is equivalent to

$$\frac{Ru^*}{\nu} = \frac{\frac{1}{2}Vd}{\nu} \frac{u^*}{V} = \frac{1}{2} \mathrm{Re}_d \left(\frac{f}{8} \right)^{1/2} \tag{6.52}$$

Introducing (6.52) and (6.51) into Eq. (6.50), changing to a base-10 logarithm, and rearranging, we obtain

$$\frac{1}{f^{1/2}} \approx 1.99 \log (\mathrm{Re}_d f^{1/2}) - 1.02 \tag{6.53}$$

In other words, by simply computing the mean velocity from the logarithmic-law correlation, we obtain a relation between the friction factor and Reynolds number for turbulent pipe flow. Prandtl derived Eq. (6.53) in 1935 and then adjusted the constants slightly to fit friction data better

$$\frac{1}{f^{1/2}} = 2.0 \log (\mathrm{Re}_d f^{1/2}) - 0.8 \tag{6.54}$$

This is the accepted formula for a smooth-walled pipe. Some numerical values may be listed as follows:

Re_d	4000	10^4	10^5	10^6	10^7	10^8
f	0.0399	0.0309	0.0180	0.0116	0.0081	0.0059

Thus f drops by only a factor of 5 over a 10,000-fold increase in Reynolds number. Equation (6.54) is cumbersome to solve if Re_d is known and f is wanted. There are many alternate approximations in the literature from which f can be computed explicitly from Re_d

$$f = \begin{cases} 0.316 \, \mathrm{Re}_d^{-1/4} & 4000 < \mathrm{Re}_d < 10^5 \quad \text{H. Blasius (1911)} \\ \left(1.8 \log \dfrac{\mathrm{Re}_d}{6.9} \right)^{-2} & \text{Ref. 9} \end{cases} \tag{6.55}$$

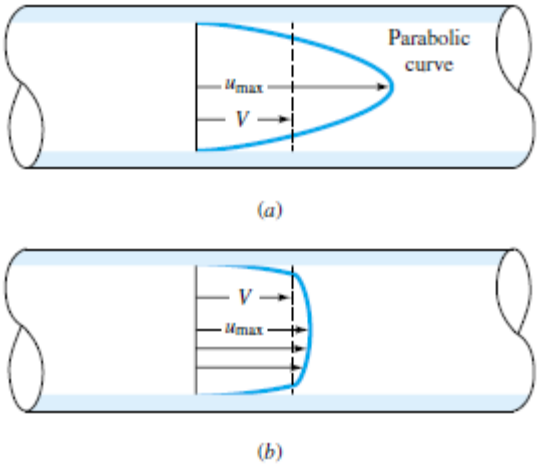

Fig. 6.11 Comparison of laminar and turbulent pipe-flow velocity profiles for the same volume flow: (*a*) laminar flow; (*b*) turbulent flow.

Chapter 6

Effect of Rough Walls

It was not known until experiments in 1800 by Coulomb [6] that surface roughness has an effect on friction resistance. It turns out that the effect is negligible for laminar pipe flow, and all the laminar formulas derived in this section are valid for rough walls also. But turbulent flow is strongly affected by roughness.

Measurements of $u(y)$ in turbulent rough-wall flow by Prandtl's student Nikuradse [7] show, as in Fig. 6.12*a*, that a roughness height ϵ will force the logarithm-law profile outward on the abscissa by an amount approximately equal to $\ln \epsilon^+$, where $\epsilon^+ = \epsilon u^*/\nu$. The slope of the logarithm law remains the same, $1/\kappa$, but the shift outward causes the constant B to be less by an amount $\Delta B \approx (1/\kappa) \ln \epsilon^+$.

Nikuradse [7] simulated roughness by gluing uniform sand grains onto the inner walls of the pipes. He then measured the pressure drops and flow rates and correlated friction factor versus Reynolds number in Fig. 6.12*b*. We see that laminar friction is unaffected, but turbulent friction, after an *onset* point, increases monotonically with the roughness ratio ϵ/d. For any given ϵ/d, the friction factor becomes constant *(fully rough)* at high Reynolds numbers. These points of change are certain values of $\epsilon^+ = \epsilon u^*/\nu$:

$$\frac{\epsilon u^*}{\nu} < 5: \quad \textit{hydraulically smooth} \text{ walls, no effect of roughness on friction}$$

$$5 \leq \frac{\epsilon u^*}{\nu} \leq 70: \quad \textit{transitional} \text{ roughness, moderate Reynolds-number effect}$$

$$\frac{\epsilon u^*}{\nu} > 70: \quad \textit{fully rough} \text{ flow, sublayer totally broken up and friction independent of Reynolds number}$$

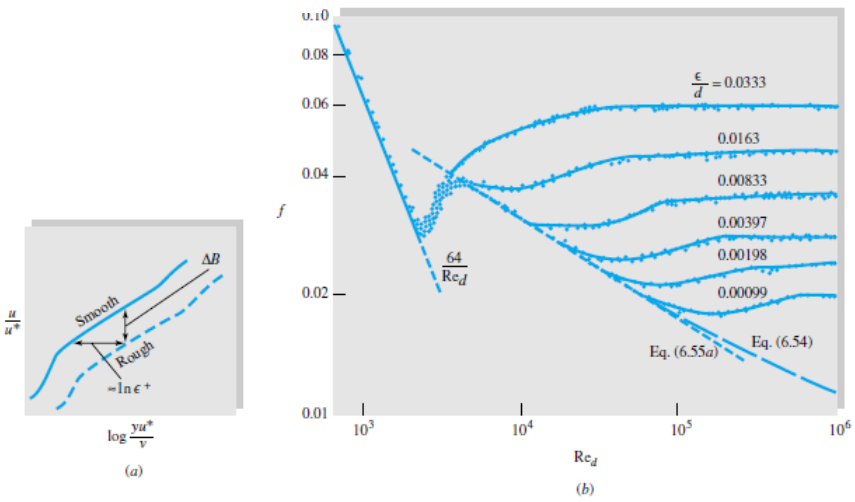

Fig. 6.12 Effect of wall roughness on turbulent pipe flow. (*a*) The logarithmic overlap-velocity profile shifts down and to the right; (*b*) experiments with sand-grain roughness by Nikuradse [7] show a systematic increase of the turbulent friction factor with the roughness ratio.

Chapter 6

The Moody Chart

In 1939 to cover the transitionally rough range, Colebrook [9] combined the smooth-wall [Eq. (6.54)] and fully rough [Eq. (6.63)] relations into a clever interpolation formula

$$\frac{1}{f^{1/2}} = -2.0 \log\left(\frac{\epsilon/d}{3.7} + \frac{2.51}{\mathrm{Re}_d f^{1/2}}\right) \tag{6.64}$$

This is the accepted design formula for turbulent friction. It was plotted in 1944 by Moody [8] into what is now called the *Moody chart* for pipe friction (Fig. 6.13). The Moody chart is probably the most famous and useful figure in fluid mechanics. It is accurate to $\pm$ 15 percent for design calculations over the full range shown in Fig. 6.13. It can be used for circular and noncircular (Sec. 6.6) pipe flows and for open-channel flows (Chap. 10). The data can even be adapted as an approximation to boundary-layer flows (Chap. 7).

Equation (6.64) is cumbersome to evaluate for f if Re_d is known, although it easily yields to the EES Equation Solver. An alternate explicit formula given by Haaland [33] as

$$\frac{1}{f^{1/2}} \approx -1.8 \log\left[\frac{6.9}{\mathrm{Re}_d} + \left(\frac{\epsilon/d}{3.7}\right)^{1.11}\right] \tag{6.64a}$$

varies less than 2 percent from Eq. (6.64).

The shaded area in the Moody chart indicates the range where transition from laminar to turbulent flow occurs. There are no reliable friction factors in this range, $2000 < \mathrm{Re}_d < 4000$. Notice that the roughness curves are nearly horizontal in the fully rough regime to the right of the dashed line.

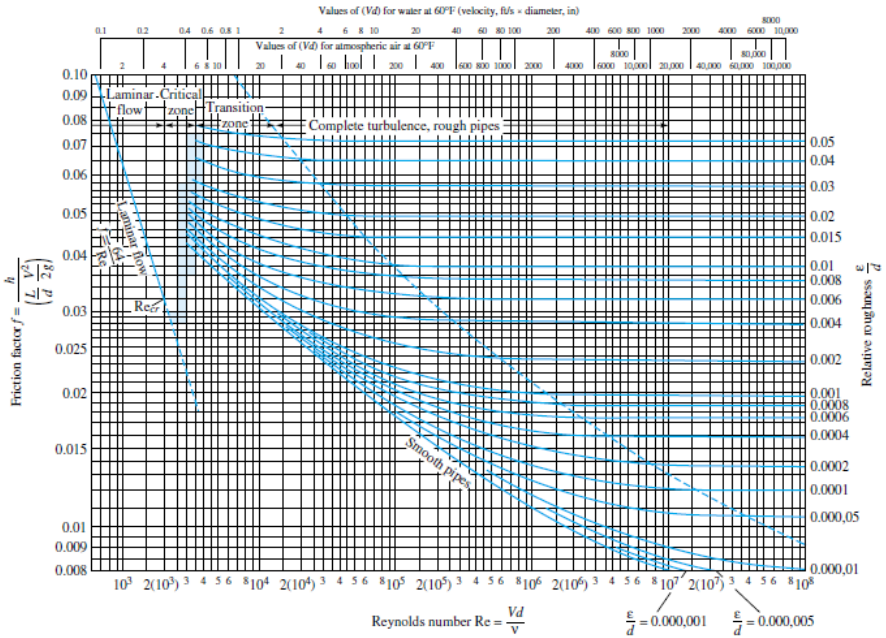

Chapter 6

Three Types of Pipe-Flow Problems

1. Given d, L, and V or Q, ρ, μ, and g, compute the head loss h_f (head-loss problem).
2. Given d, L, h_f, ρ, μ, and g, compute the velocity V or flow rate Q (flow-rate problem).
3. Given Q, L, h_f, ρ, μ, and g, compute the diameter d of the pipe (sizing problem).

Only problem 1 is well suited to the Moody chart. We have to iterate to compute velocity or diameter because both d and V are contained in the ordinate *and* the abscissa of the chart.

Type 2 Problem: Find the Flow Rate

Even though velocity (or flow rate) appears in both the ordinate and the abscissa on the Moody chart, iteration for turbulent flow is nevertheless quite fast, because f varies so slowly with Re_d. Alternately, in the spirit of Example 5.7, we could change the scaling variables to (ρ, μ, d) and thus arrive at dimensionless head loss versus dimensionless *velocity*. The result is[4]

$$\zeta = \text{fcn}(\mathrm{Re}_d) \qquad \text{where} \qquad \zeta = \frac{g d^3 h_f}{L\nu^2} = \frac{f\,\mathrm{Re}_d^2}{2} \tag{6.65}$$

Example 5.7 did this and offered the simple correlation $\zeta \approx 0.155\ \mathrm{Re}_d^{1.75}$, which is valid for turbulent flow with smooth walls and $\mathrm{Re}_d \le 1$ E5.

A formula valid for all turbulent pipe flows is found by simply rewriting the Colebrook interpolation, Eq. (6.64), in the form of Eq. (6.65):

$$\mathrm{Re}_d = -(8\zeta)^{1/2} \log\left(\frac{\epsilon/d}{3.7} + \frac{1.775}{\sqrt{\zeta}}\right) \qquad \zeta = \frac{g d^3 h_f}{L\nu^2} \tag{6.66}$$

Given ζ, we compute Re_d (and hence velocity) directly.

Type 3 Problem: Find the Pipe Diameter

The Moody chart is especially awkward for finding the pipe size, since d occurs in all three parameters f, Re_d, and ϵ/d.

simply set up the problem as an iteration in terms of the Moody-chart variables.

First write the diameter in terms of the friction factor:

$$f = h_f \frac{d}{L}\frac{2g}{V^2} = \frac{\pi^2}{8}\frac{g h_f d^5}{L Q^2} \quad (1) \qquad (2) \qquad (3)$$

Also write the Reynolds number and roughness ratio in terms of the diameter: $\mathrm{Re}_d = \dfrac{Vd}{\nu} = \dfrac{4Q}{\pi d \nu}$; $\dfrac{\epsilon}{d}$

Guess f, compute d from (1), then compute Re_d from (2) and ϵ/d from (3), and compute a better f from the Moody chart or Eq. (6.64). Repeat until (fairly rapid) convergence.

Chapter 6

The Hydraulic Diameter

For a noncircular duct, the control-volume concept of Fig. 6.10 is still valid, but the cross-sectional area A does not equal πR^2 and the cross-sectional perimeter wetted by the shear stress $\mathcal{P}$ does not equal $2\pi R$. The momentum equation (6.26) thus becomes

$$\Delta p\, A + \rho g A\, \Delta L \sin\phi - \bar{\tau}_w \mathcal{P}\, \Delta L = 0$$

or

$$h_f = \frac{\Delta p}{\rho g} + \Delta z = \frac{\bar{\tau}_w}{\rho g}\frac{\Delta L}{A/\mathcal{P}} \tag{6.70}$$

This is identical to Eq. (6.27) except that (1) the shear stress is an average value integrated around the perimeter and (2) the length scale $A/\mathcal{P}$ takes the place of the pipe radius R. For this reason a noncircular duct is said to have a *hydraulic radius* R_h, defined by

This concept receives constant use in open-channel flow (Chap. 10), where the channel cross section is almost never circular. If, by comparison to Eq. (6.29) for pipe flow, we define the friction factor in terms of average shear

$$f_{\text{NCD}} = \frac{8\bar{\tau}_w}{\rho V^2} \tag{6.72}$$

where NCD stands for noncircular duct and $V = Q/A$ as usual, Eq. (6.70) becomes

$$h_f = f\frac{L}{4R_h}\frac{V^2}{2g} \tag{6.73}$$

This is equivalent to Eq. (6.30) for pipe flow except that d is replaced by $4R_h$. Therefore we customarily define the *hydraulic diameter* as

$$D_h = \frac{4A}{\mathcal{P}} = \frac{4 \times \text{area}}{\text{wetted perimeter}} = 4R_h \tag{6.74}$$

We should stress that the wetted perimeter includes all surfaces acted upon by the shear stress. For example, in a circular annulus, both the outer and the inner perimeter should be added. The fact that D_h equals $4R_h$ is just one of those things: Chalk it up to an engineer's sense of humor. Note that for the degenerate case of a circular pipe, $D_h = 4\pi R^2/(2\pi R) = 2R$, as expected.

We would therefore expect by dimensional analysis that this friction factor f, based upon hydraulic diameter as in Eq. (6.72), would correlate with the Reynolds number and roughness ratio based upon the hydraulic diameter

$$f = F\left(\frac{VD_h}{\nu}, \frac{\epsilon}{D_h}\right) \tag{6.75}$$

and this is the way the data are correlated. But we should not necessarily expect the Moody chart (Fig. 6.13) to hold exactly in terms of this new length scale. And it does not, but it is surprisingly accurate:

$$f \approx \begin{cases} \dfrac{64}{\text{Re}_{D_h}} & \pm 40\% \quad \text{laminar flow} \\ f_{\text{Moody}}\left(\text{Re}_{D_h}, \dfrac{\epsilon}{D_h}\right) & \pm 15\% \quad \text{turbulent flow} \end{cases} \tag{6.76}$$

Chapter 6

6.7 Minor Losses in Pipe Systems[7]

For any pipe system, in addition to the Moody-type friction loss computed for the length of pipe, there are additional so-called *minor losses* due to

1. Pipe entrance or exit
2. Sudden expansion or contraction
3. Bends, elbows, tees, and other fittings
4. Valves, open or partially closed
5. Gradual expansions or contractions

The measured minor loss is usually given as a ratio of the head loss $h_m = \Delta p/(\rho g)$ through the device to the velocity head $V^2/(2g)$ of the associated piping system

$$\text{Loss coefficient } K = \frac{h_m}{V^2/(2g)} = \frac{\Delta p}{\frac{1}{2}\rho V^2} \tag{6.98}$$

A single pipe system may have many minor losses. Since all are correlated with $V^2/(2g)$, they can be summed into a single total system loss if the pipe has constant diameter

$$\Delta h_{tot} = h_f + \sum h_m = \frac{V^2}{2g}\left(\frac{fL}{d} + \sum K\right) \tag{6.100}$$

Note, however, that we must sum the losses separately if the pipe size changes so that V^2 changes. The length L in Eq. (6.100) is the total length of the pipe axis, including any bends.

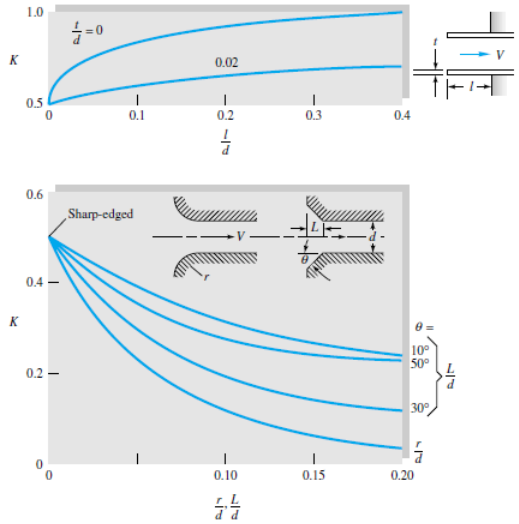

Fig. 6.21 Entrance and exit loss coefficients: (*a*) reentrant inlets; (*b*) rounded and beveled inlets. Exit losses are $K \approx 1.0$ for all shapes of exit (reentrant, sharp, beveled, or rounded). *(From Ref. 37.)*

Table 6.5 Resistance Coefficients $K = h_m/[V^2/(2g)]$ for Open Valves, Elbows, and Tees

	Nominal diameter, in								
	Screwed				Flanged				
	½	1	2	4	1	2	4	8	20
Valves (fully open):									
Globe	14	8.2	6.9	5.7	13	8.5	6.0	5.8	5.5
Gate	0.30	0.24	0.16	0.11	0.80	0.35	0.16	0.07	0.03
Swing check	5.1	2.9	2.1	2.0	2.0	2.0	2.0	2.0	2.0
Angle	9.0	4.7	2.0	1.0	4.5	2.4	2.0	2.0	2.0
Elbows:									
45° regular	0.39	0.32	0.30	0.29					
45° long radius					0.21	0.20	0.19	0.16	0.14
90° regular	2.0	1.5	0.95	0.64	0.50	0.39	0.30	0.26	0.21
90° long radius	1.0	0.72	0.41	0.23	0.40	0.30	0.19	0.15	0.10
180° regular	2.0	1.5	0.95	0.64	0.41	0.35	0.30	0.25	0.20
180° long radius					0.40	0.30	0.21	0.15	0.10
Tees:									
Line flow	0.90	0.90	0.90	0.90	0.24	0.19	0.14	0.10	0.07
Branch flow	2.4	1.8	1.4	1.1	1.0	0.80	0.64	0.58	0.41

Chapter 6

Multiple-Pipe Systems

Figure 6.24 shows three examples of multiple-pipe systems. The first is a set of three (or more) pipes in series. Rule 1 is that the flow rate is the same in all pipes

$$Q_1 = Q_2 = Q_3 = \text{const}$$

or

$$V_1 d_1^2 = V_2 d_2^2 = V_3 d_3^2 \tag{6.105}$$

Rule 2 is that the total head loss through the system equals the sum of the head loss in each pipe

$$\Delta h_{A\to B} = \Delta h_1 + \Delta h_2 + \Delta h_3 \tag{6.106}$$

The second multiple-pipe system is the *parallel*-flow case shown in Fig. 6.24*b*. Here the loss is the same in each pipe, and the total flow is the sum of the individual flows

$$\Delta h_{A\to B} = \Delta h_1 = \Delta h_2 = \Delta h_3 \tag{6.109a}$$

$$Q = Q_1 + Q_2 + Q_3 \tag{6.109b}$$

Consider the third example of a *three-reservoir pipe junction*, as in Fig. 6.24*c*. If all flows are considered positive toward the junction, then

$$Q_1 + Q_2 + Q_3 = 0 \tag{6.110}$$

which obviously implies that one or two of the flows must be away from the junction. The pressure must change through each pipe so as to give the same static pressure p_J at the junction. In other words, let the HGL at the junction have the elevation

$$h_J = z_J + \frac{p_J}{\rho g}$$

where p_J is in gage pressure for simplicity. Then the head loss through each, assuming $p_1 = p_2 = p_3 = 0$ (gage) at each reservoir surface, must be such that

$$\Delta h_1 = \frac{V_1^2}{2g}\frac{f_1 L_1}{d_1} = z_1 - h_J$$

$$\Delta h_2 = \frac{V_2^2}{2g}\frac{f_2 L_2}{d_2} = z_2 - h_J \tag{6.111}$$

$$\Delta h_3 = \frac{V_3^2}{2g}\frac{f_3 L_3}{d_3} = z_3 - h_J$$

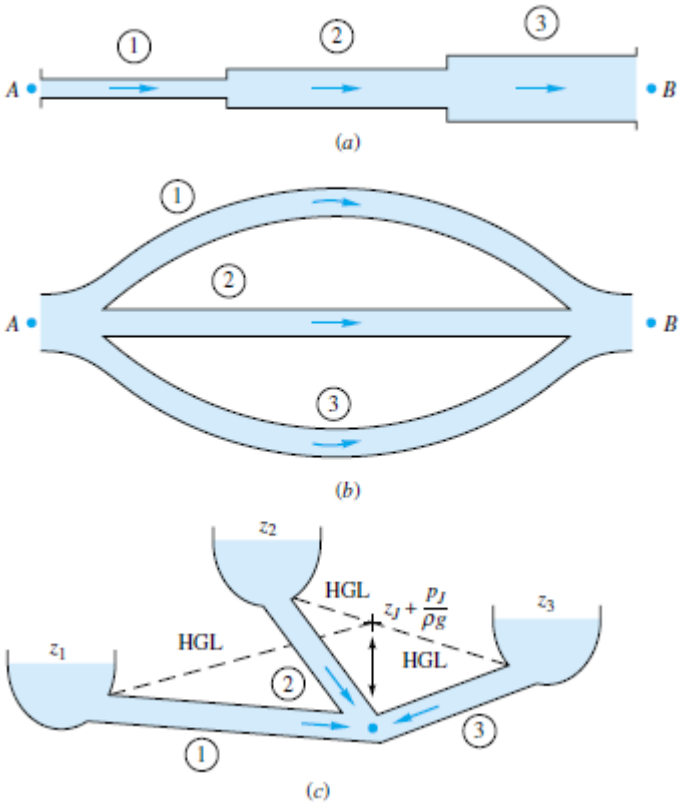

Fig. 6.24 Examples of multiple-pipe systems: (*a*) pipes in series; (*b*) pipes in parallel; (*c*) the three-reservoir junction problem.

Chapter 6

Multiple-Pipe Systems

The ultimate case of a multipipe system is the *piping network* illustrated in Fig. 6.25. This might represent a water supply system for an apartment or subdivision or even a city. This network is quite complex algebraically but follows the same basic rules:

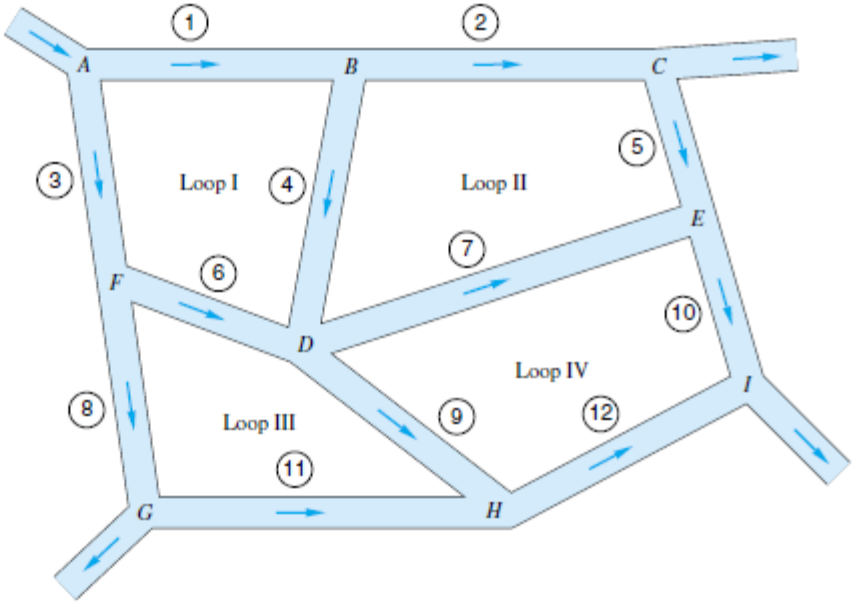

Fig. 6.25 Schematic of a piping network.

1. The net flow into any junction must be zero.
2. The net head loss around any closed loop must be zero. In other words, the HGL at each junction must have one and only one elevation.
3. All head losses must satisfy the Moody and minor-loss friction correlations.